Journal of Molecular Catalysis A: Chemical 353–354 (2012) 163–170

Contents lists available at SciVerse ScienceDirect

Journal of Molecular Catalysis A: Chemical

journal homepage: www.elsevier.com/locate/molcata

Rapid microwave-assisted synthesis of one-dimensional silver–$H_2Ti_3O_7$ nanotubes

V. Rodríguez-González[a,*], S. Obregón-Alfaro[b], L.M. Lozano-Sánchez[a], Soo-Wohn Lee[c]

[a] IPICYT, Instituto Potosino de Investigación Científica y Tecnológica, División de Materiales Avanzados, Camino a la Presa San José 2055 Col. Lomas 4a. sección C.P. 78216, San Luis Potosí, S.L.P., Mexico
[b] Instituto de Ciencia de Materiales de Sevilla, Centro Mixto Universidad de Sevilla-CSIC, C/Américo Vespucio 49, 41092 Sevilla, Spain
[c] Global Research Laboratory, Sun Moon University, Galsan-Ri, Tangjung-Myon, Asan Chungnam 336-708, South Korea

ARTICLE INFO

Article history:
Received 12 September 2011
Received in revised form
14 November 2011
Accepted 15 November 2011
Available online 23 November 2011

Keywords:
Nanocrystalline silver–TiO_2
Microwave-assisted synthesis
Photocatalytic activity
$H_2Ti_3O_7$ nanotubes
TiO_2 nanoribbons

ABSTRACT

The formation of silver hydrogen trititanate nanotubes, based on the controllable microwave-assisted hydrothermal nanocrystalline TiO_2 transition, was investigated by means of XRD, UV–vis–DRS, Raman, FESEM and HRTEM. The results show that the rapid formation of H-trititanate nanotubes is achieved by self-assemblage of silver nanoparticles in which the lamellar intermediates react with NaOH in hydrothermal conditions. The presence of Ag° nanoparticles in the precursor promotes rapid and more complete formation of layered $H_2Ti_3O_7$ nanotubes. After reacting for 4 h without subsequent thermal treatment, the inner diameters of the cylinder-like nanotubes are in the range of 3.6–4.0 nm, while their outer diameters are in the range of 7.6–8 nm. In addition, some straight nanotubes form bundles which are hundreds of nanometers in length. As-synthesized ultrathin nanotubes and crystalline precursors were evaluated by methyl orange dye (MOD) UV photo-oxidation. The complete degradation of MOD is achieved after 3.5 h of UV irradiation in the presence of silver–TiO_2 nanocomposites, resulting in 50% of dye mineralization.

1. Introduction

Synthesis and tailoring of the structures of semiconductors based on nanocrystalline TiO_2 have received considerable attention due to their unique physical and chemical properties and their potential applications in industry and technology [1–3]. One of the most studied TiO_2 applications is in the area of photocatalysis, which has led to their use as efficient detoxification or remediation, mineralization, and disinfection agents of wastewater. The photocatalysis is a well-known technique in the treatment of wastewater [3,4]. Many modifications of the TiO_2 semiconductor have been studied with the aim of enhancing the activity and stability of these materials and of extending these photochemical applications with TiO_2 into the visible region of the spectrum for wastewater treatment applications [5]. While various methods have been used to synthesize titanium dioxide nanoparticles, such as anodization process [6–8], combustion [9], and sol–gel techniques [10], hydrothermal synthesis in alkaline solution has proved to be a particularly attractive approach for the preparation of 1-D nanostructures of TiO_2. This is because the method uses only a few reagents, produces relatively pure materials, and the process is simple and inexpensive [11–18].

The oxidation of organic contaminants of wastewater appears to rely on a surface phenomenon to achieve mineralization. This phenomena has been studied by heterogeneous photocatalysis that focuses on the study of photoassisted reactions using an irradiated nanostructured semiconductor as the photocatalyst [2,3]. The photocatalyst may be modified in many ways: by doping with transition metals, rare earth metals, functionalization by impregnation or deposition of noble metal atoms, photosensitization with dyes, sulfates, and modification of the structures by reactions such as the sol–gel, or the hydrothermal process.

The aim of this research is to study how to tailor the physical, chemical, structural, and photocatalytic properties of the silver–$H_2Ti_3O_7$ material prepared by a simple, inexpensive, and rapid hydrothermal treatment using microwave irradiation.

In this work, titanate nanotubes were shown to be effective support matrices for the immobilization of silver nanoparticles. As a result, we also report a comparative study with the corresponding analogue nanocrystalline anatase TiO_2 to understand the synthesis and the properties of these two nanostructures and to evaluate their activity in the photocatalytic degradation of methyl orange dye under UV Light irradiation.

* Corresponding author. Tel.: +52 44 8342000x7295.
E-mail address: vicente.rdz@ipicyt.edu.mx (V. Rodríguez-González).

1381-1169/$ – see front matter © 2011 Elsevier B.V. All rights reserved.
doi:10.1016/j.molcata.2011.11.020

2. Experimental

2.1. Preparation of silver photo-deposited TiO_2

For photochemical deposition of silver nanoparticles on titanium dioxide, the P25 Degussa material (75% anatase, 25% rutile) was used as a TiO_2 precursor. First, 0.472 g of silver nitrate (Samchun, 99.8%) were added to 1 L of distilled water and placed in an ultrasonic bath for 5 min to assure the complete dissolution of silver precursor particles. Then, 29.7 g of TiO_2 (P25 Degussa) were added to the aqueous solution and the slurry was maintained for 1 h under continuous magnetic stirring to achieve adsorption equilibrium of the Ag^+ ions on the TiO_2 surface. Afterwards, the mixture was exposed to UV light with two 20 W UV C-type lamps (Black light lamp-BL, Sankyo Denky, Japan) for 2 h. Then, the slurry was transferred to a vacuum rotary evaporator and dried at 80 °C for 4 h. The final powder was heated at 100 °C overnight. The so-obtained powder is referred to as Nc-STPD.

2.2. Synthesis of silver–TiO_2 nanocomposite by the sol–gel method

The silver–TiO_2 sample was prepared by sol–gel method by adding dropwise 130.36 g of titanium *n*-butoxide (Sigma–Aldrich, 97%), 53 mL of *n*-butanol, and 28 mL of a 0.1 M silver aqueous solution (silver nitrate, Samchun, 99.8%) to 53 mL of butanol–28 mL water solution contained in a 4-neck round bottom flask (1 L) equipped with a thermometer. The butoxide/*n*-butanol/water molar ratio was 1/3/8 and the final amount of silver was 1 wt%. The slurry was maintained in the dark under magnetic stirring at 80 °C for 4 h. The gelled product was aged for 72 h. The solvents and unreacted precursors were removed in a vacuum evaporator at 80 °C, dried overnight under vacuum at 100 °C, and calcined at 450 °C for 4 h. The so-obtained powder is referred to as Nc-STSG.

2.3. Silver–$H_2Ti_3O_7$ nanotubes synthesis

Two grams of silver–TiO_2 sample were suspended in 100 mL of 10 M NaOH aqueous solution. The slurry was placed in an ultrasonic bath for 5 min to eliminate aggregates and then stirred for 10 min at room temperature. The mixture was placed in a Teflon vessel and heated by microwave irradiation in a microwave reactor (Eyela MWO-1000 Wave Magic) at 150 °C for 4 h, 400 rpm and a maximum variable microwave irradiation power of 195 W. Afterwards, the obtained material was cooled to room temperature and neutralized with 5 N HCl. Then, the resulting powder was washed thoroughly with distilled water until the pH of the washing solution was ~7. The powder was filtered and dried at 95 °C for 12 h. The obtained powder is referred to as Nt-STSG for nanotubes from silver TiO_2 sol–gel precursor and as Nt-STPD for nanotubes from the silver photodeposited TiO_2 precursor. P25 Degussa material (75% anatase, 25% rutile) was used as a TiO_2 precursor for the synthesis of $H_2Ti_3O_7$ nanotubes in identical conditions, but without the presence of silver referred to as Nt–TiO_2.

2.4. Characterization of silver TiO_2 nanocrystalline structures

All samples were stored at room temperature inside a vacuum desiccator, away from light in order to prevent light induced modifications. The crystalline phases were determined by X-ray diffraction (XRD) with a Bruker D8 Advance diffractometer using CuKα radiation (λ = 1.5 Å). Optical characterization of the semiconductors was performed with a Varian Cary 100 UV–Vis (diffuse reflectance) spectrophotometer, equipped with an integrating sphere. In order to estimate the energy band gap (e.g.; electronic transitions) of the catalysts, the equipment was calibrated with a Spectralon standard (Labsphere SRS-99-010, 99% reflectance). Then, the band gap of the solids was calculated by linearization of the UV spectra to the *X* axis (wavelength in nm) for *Y* axis (absorbance) equal to zero for indirect allowed transitions. The Raman spectra were recorded on a Renishaw MicroRaman Invia Spectrometer, equipped with an Argon laser source. The laser excitation line was 514 nm and the power was 25 mW.

FESEM images were obtained by means of a Helios NanoLab 600i equipped with Advanced DualBeam for ultra-high resolution imaging. The HRTEM and HAADF-STEM images were obtained with a FEI Tecnai F30 Super-win equipped with a LaB6 emission gun operating at 300 kV. The point to point resolution is 0.24 nm; and the information limit is 0.14 nm. The HRTEM digital images were obtained with a CCD camera and the Digital Micrograph Software from GATAN. The elemental composition of the samples was determined by energy dispersive X-ray spectroscopy (EDS) with an EDAX spectrometer fitted to the TEM. The powdered samples were ultrasonically dispersed in isopropyl alcohol and supported on holey carbon coated copper grids. The particle size and nanotube diameter distribution histograms for the samples were established from the measurements of 200–300 particles. The average particle diameter was calculated by using the following formula: $ds = \Sigma nidi/\Sigma ni$, where *ni* is the number of particles of diameter *di*.

2.5. Experimental procedure of photocatalytic degradation of methyl orange dye

The photocatalytic degradation of methyl orange dye (Methyl Orange A.C.S, Aldrich), was performed with a standard Pen-Ray UV lamp (UVP Products) with a typical intensity of 4400 μW/cm^2 at 254 nm. The photocatalytic tests were performed in a slurry home-made reactor at room temperature. The quartz lamp was immersed in a cooled vessel containing the reactant solution consisting of 250 mL with 35 ppm of MOD and 250 mg of catalyst. In order to achieve the saturation of dissolved oxygen and to assure the adsorption–desorption equilibrium of MOD on the semiconductor, the dry air was bubbled for 30 min (30 mL min^{-1}) into the suspension under gentle magnetic stirring (240 rpm) before turning on the light source. The photodegradation rate was obtained by following the intensity of the MOD absorption band at 465 nm as a function of the irradiation time. Aliquots of the irradiated solution were filtered through a 0.45 μm nylon filter and monitored with a Varian Cary 100 UV–vis spectrophotometer. All of the photocatalytic experiments were repeated at least twice. Estimated errors did not exceed 3.0%.

3. Results and discussion

3.1. XRD analysis

XRD patterns obtained after microwave treatment show that the crystallinity of titanate nanotubes is generally poor (see Fig. 1). Reflections are marked as R, A and T corresponding to the rutile TiO_2 phase (JCPDS 21-1276), TiO_2 anatase phase (JCPDS 21-1272) and the titanate phase nanotubes $H_2Ti_3O_7$ (JCDPS 36-654). In addition, a small peak at 30.83 of 2θ is observed for sol–gel nanocrystalline sample (Nc-STSG), which may be assigned to the brookite TiO_2 phase (JCPDS 76-1934).

However, according to the XRD patterns a complete phase transition was achieved for both silver TiO_2 nanocrystalline precursors of titanate nanotubes. The titanate nanotubes obtained from TiO_2 Degussa precursor have much less intensity, Nt–TiO_2 than Nt–ST samples. All of the reflections in the titanate nanotubes have broad profiles which could be attributed to hydrogen trititanate nanotubes phase $H_2Ti_3O_7$ (JCDPS 36-654) [15–18]. The presence of

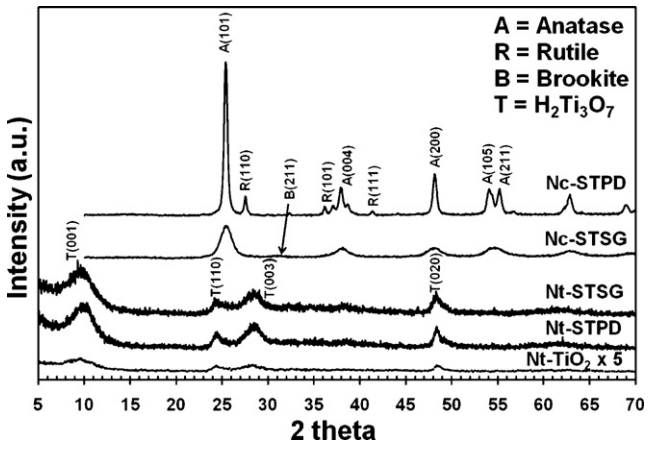

Fig. 1. Powder XRD patterns of the synthesized silver TiO_2 nanocrystalline and silver $H_2Ti_3O_7$ nanotubes.

Ag° nanoparticles in the precursor would cause the rapid and more complete formation of layered $H_2Ti_3O_7$ nanotubes compared to bare TiO_2 nanotubes. Evidence for the new one-dimensional titanate nanostructure ($H_2Ti_3O_7$) may be suggested by the ordered structure of nano-crystalline TiO_2 during the microwave process, being consistent with the literature [18]. Fig. 1 shows that with only 4 h of irradiation under alkaline conditions at 150 °C, all reflections of the silver nanotubes are attributed to pure hydrogen trititanate nanotubes. Similar XRD patterns have been reported under similar conditions [18]. However, longer microwave irradiation time was used [18] or sodium atoms remain in the one-dimensional titanate nanotube [11,19]. Also, doping titanates with exchangeable ions may help to obtain the pure hydrogen trititanate nanotubes [13,15,16]. The formation of nanotubes is independent from the original structure of TiO_2 [24]. However, the presence of the silver nanoparticles on the TiO_2 precursor may favor and catalyze the formation of the final trititanate nanotubes. Peaks attributed to silver particles (Ag° or AgO_x) were not identified and therefore it may be assumed that some Ag^{+} ions may be inserted into the framework of titanium dioxide for the sol–gel sample or deposited in nanometer size on the TiO_2 surface for the deposited samples and the titanate nanostructures. However, the size of such silver nanoparticles is below the resolution of the diffractometer. Other related studies indicating the presence of cations, for example Zn^{2+}, in hydrothermal treatment would cause the formation of layered $H_2Ti_2O_5(H_2O)$ nanosheets [13].

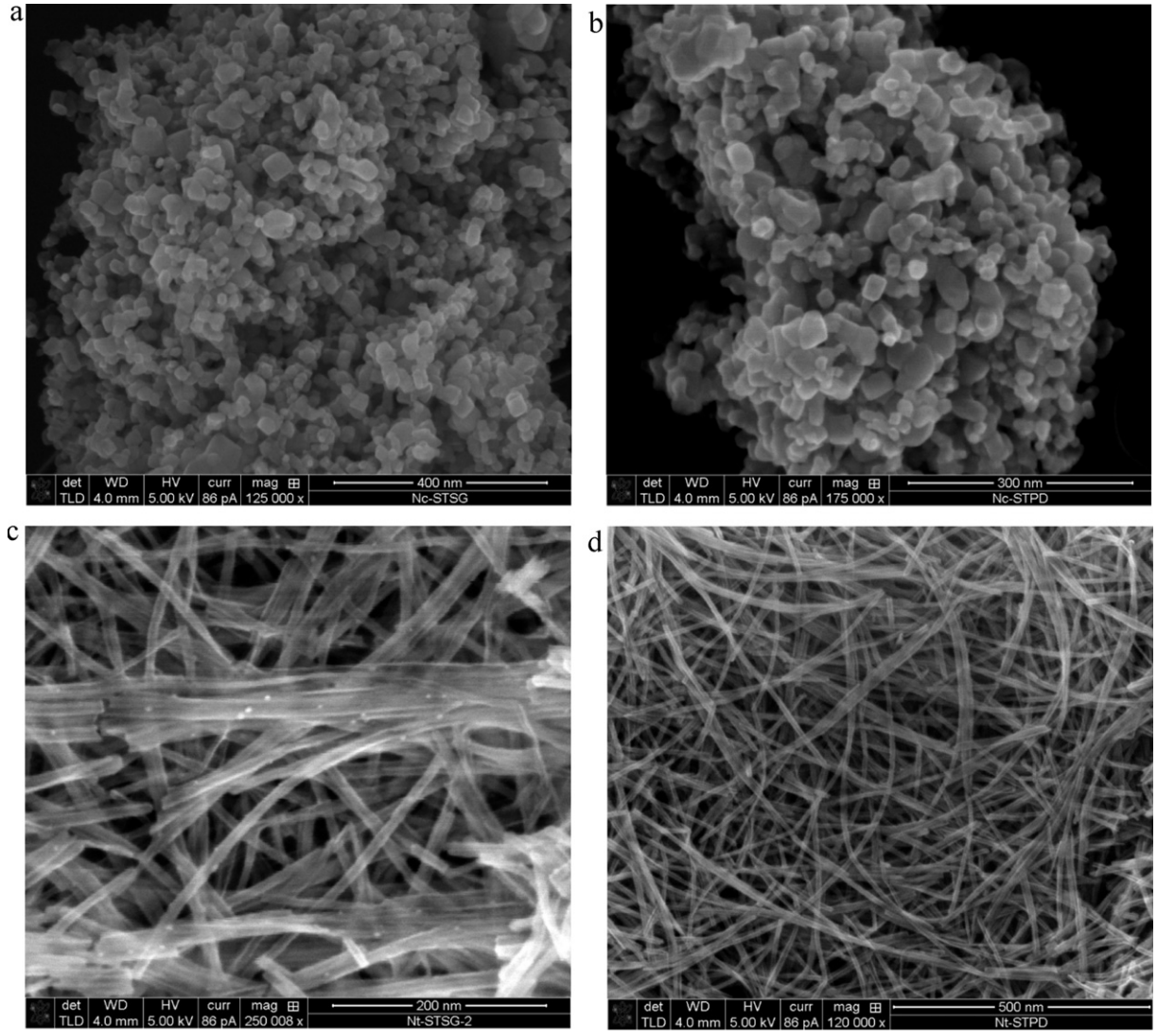

Fig. 2. FESEM images obtained for the (a) Nc-STSG, (b) Nc-STPD, (c) Nt-STSG, and (d) Nt-STPD powders.

3.2. FESEM and HRTEM observation

The morphologies of the hydrogen trititanate nanotubes and nanocrystalline precursors were analyzed by FESEM, Fig. 2a–d. The nanocrystalline TiO_2 prepared by sol–gel (Nc-STSG) precursor consists of faceted rectangular and quasi-spherical particles of ~20 nm in diameter (Fig. 2a). The precursor prepared by silver photodeposition on commercial TiO_2, Nc-STPD, shows similar morphology but with crystalline particles of ~28 nm in diameter (Fig. 2b). The FESEM images obtained for the one-dimensional Nt-STSG, and Nt-STPD powders, are shown in Fig. 2c and d, where the formation of nanotubes is observed. The diameter of Nt-STSG is 4–10 nm, with a length of ~400 to 600 nm. On the other hand, for the Nt-STPD the formation of ultrathin nanotubes was observed (~6 nm in diameter). It can also be noted that in the Nt-STPD powder, the lengths of nanotubes are twice those of the Nt-STSG preparations (~0.8 to 1 μm). In addition, we observe some silver nanoparticles formed on the surfaces of the titanate nanotubes. In the literature, the trititanate nanotubes exhibit diameters of about 11 nm and length of several ten to several hundreds nanometers, respectively [18].

The hydrogen trititanate nanotubes obtained in the present work are pure and ultrathin (8 nm) compared to other reports in the literature [11,12,15]. FESEM images of silver TiO_2 nanotubes illustrate (Fig. 2c and d) that the Nt-STPD nanotubes seem to be more oriented and also that silver nanoparticles are not observed, perhaps because nanoparticles are highly dispersed on the surface and some nanoparticles are lixiviated during the transformation process. In Nt-STSG obtained from sol–gel preparations, the nanotubes are interwoven (Fig. 2d) and silver nanoparticles are observed on the surface of protonated nanotubes. FESEM images shows that the nanotubes obtained from photodeposited silver TiO_2-P25 are larger than those from Nt-STSG. When the silver–TiO_2 precursor is more nanocrystalline, larger and thinner nanotubes are obtained [14]. Nanocrystalline P25 TiO_2 with 27 nm crystallite size seems to be nanotubes in a more complete way.

HRTEM observations of Nt-STSG Fig. 3a indicate that the nanotubes are generally three to four layered with an interlayer separation of ~0.74 nm. HRTEM observations reveal that the titanate nanotubes have almost uniform inner diameters of ~3.4 nm and outer diameters of ~9.1 nm. A few unrolling layers are observed which suggests a lamellar intermediate phase in the mechanism of the transformation of the nanocrystalline precursor Fig. 3a [13]. This is important for the mechanisms of formation of nanotubes from TiO_2 crystallites reported previously [11,14,18,20]. The mechanism of formation of nanotubes from TiO_2 anatase in alkaline ambient is described elsewhere in the literature [14]. In brief, the alkaline environment causes dissolution of the TiO_2, and a reprecipitation as layered titanate occurs. From these layered structures, nanotubes are formed because of the asymmetric environment caused by mechanical stress (hydrothermal environment). Recrystallization of trititanate nanotubes yielded it as a final product in a complete transformation [14]. Also, recrystallizations of anatase and rutile phases are possible [15,18,21,22].

For Nt-STPD the interlayer separation is ~0.8 nm [14,18], which suggests that the layers are least compact perhaps because the interlayer and length are greater than that in Nt-STSG. The titanate nanotubes have outer diameters of ca. ~8 nm and inner diameters of 3.6 nm, with the wall being composed of three or four stacked layers. These nanotubes seem to be less rigid perhaps because of their greater length. Also, a few layers seem to be unrolled (to form nanoribbons-like) and some nanotubes were not well rolled (scroll-like) by these preparations (see Fig. 4a and b. In Fig. 3a and b, some silver nanoparticles are observed to have been

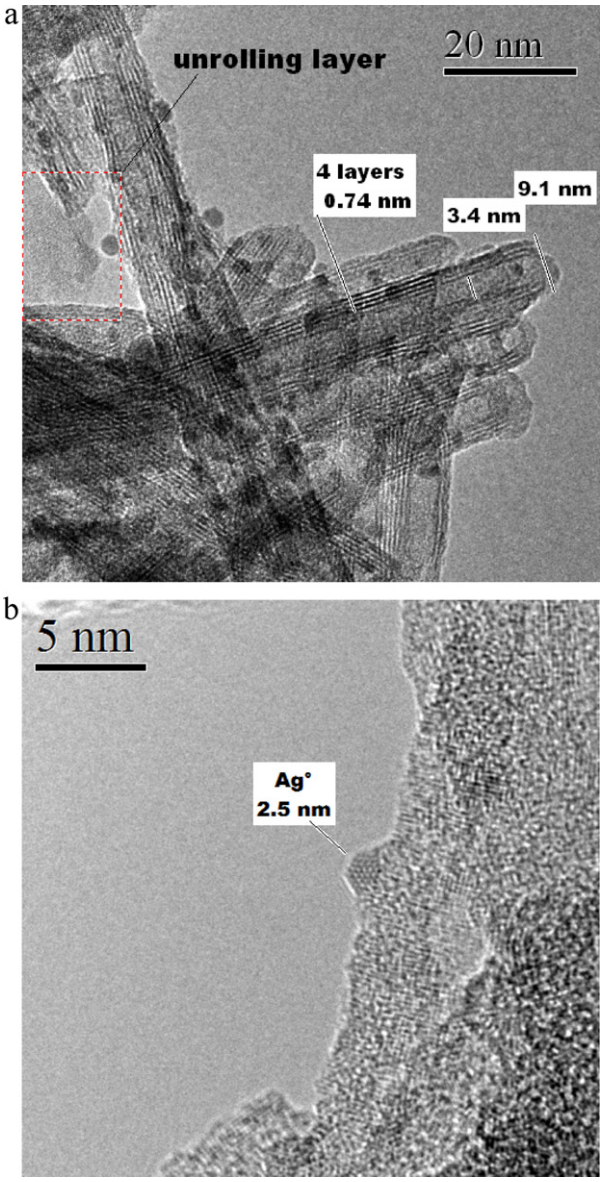

Fig. 3. (a, b) HRTEM images for Nt-STSG.

deposited preferentially over the outer diameter with an average nanoparticle size of 2.7 nm.

In Fig. 3b, metallic silver nanoparticles of 2.5 nm were detected, with an interplanar separation of 0.235 nm which is close to the interplanar distance in the cubic metallic silver phase (1 1 1) and with hexagonal shape [11]. HRTEM observations suggest that the silver nanoparticles from silver doped TiO_2, prepared by sol–gel method, were segregated on the surface of titanate nanotubes during the transformation process. Due to the low content of silver, it is difficult to observe the nanoparticles even by high-angle annular dark-field-scanning transmission electronic microscopy (HAADF-STEM). According to XRD, the silver nanoparticles may be either highly dispersed on the nanotube surface or some particles are lixiviated during the microwave transformation. Previous work using the HAADF-STEM mode detected an average nanoparticle size of 4.5 nm for Nc-STPD and 2.0 nm for the Nc-STSG [23]. It was reported that when the nanocrystalline precursor is transformed to one-dimensional hydrogen trititanate nanotubes, the surface area increases to $\geq 200\ m^2/g$ [11,18]. As a result, the silver nanoparticles are possibly highly monodispersed and difficult to characterize by XRD, even with HRTEM or HAADF-STEM.

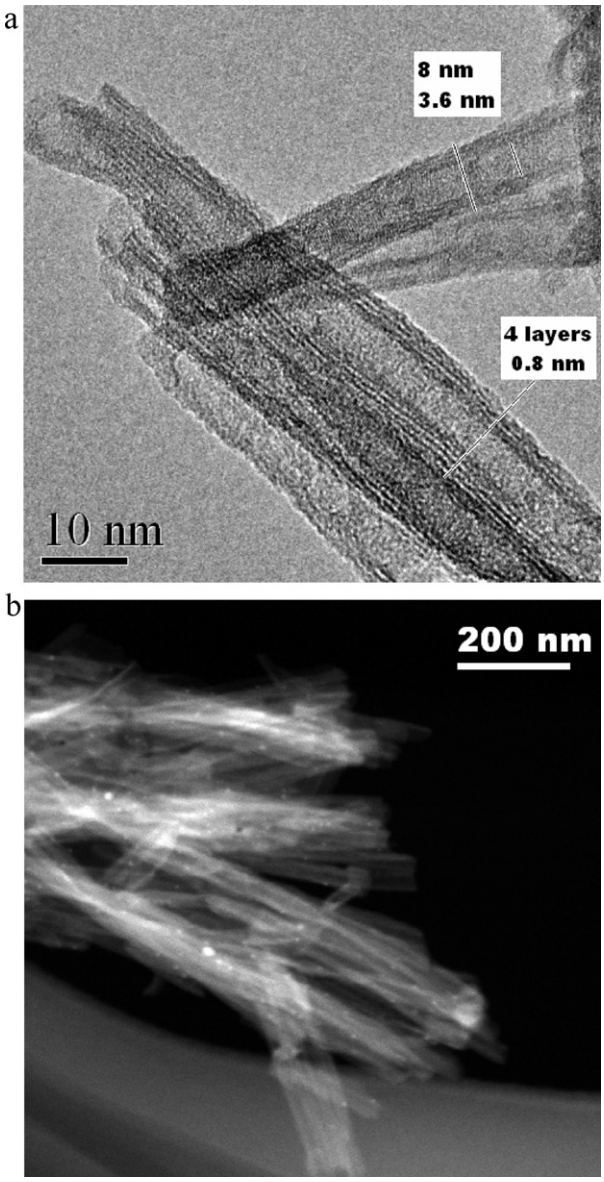

Fig. 4. (a, b) HRTEM and HAADF images for Nt-STPD.

The $H_2Ti_3O_7$ with analogous nanotube morphology to that obtained in the present work was reported by Qing et al. [24]. They prepared $Na_2Ti_3O_7$ by a hydrothermal method. Thin titanate fibers with a diameter of 50 nm and lengths up to several micrometers were reported [24]. Thin nanowires with diameter of 65 nm have been synthesized by treating brookite and anatase nanocrystallites in a 10 M NaOH aqueous solution under hydrothermal conditions, 180 °C for more than 12 days [25]. Toledo-Antonio et al. [11] transformed TiO_2 anatase into TiO_2 nanotubes by hydrothermal treatment for 18 h at 100 °C then decorated with silver nanoparticles by aqueous ion exchange in special acidic conditions and with subsequent N_2 annealing conditions for 4 h. Silver nanoparticles are characterized by HAADF-STEM in support resulting in quasi-monodisperse Ag nanoparticles of an average size of 5 nm [11]. In this research, we have obtained more ultrathin $H_2Ti_3O_7$ nanotubes with silver nanoparticles on the surface of 4 nm in average in only 4 h. Other's studies reported that the formation kinetics of TNTs was enhanced using microwave-assisted hydrothermal treatment [13]

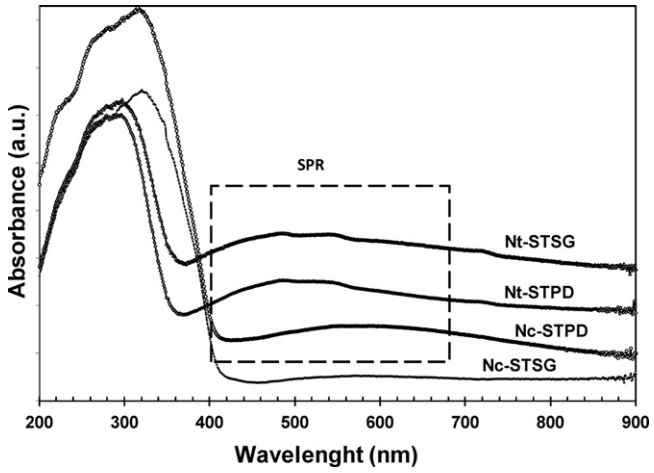

Fig. 5. Diffuse reflectance spectra of silver nanocrystalline and nanotube composites.

3.3. UV–vis spectra.

Fig. 5 shows the UV–vis diffuse reflectance spectra of TiO_2 silver nanocrystalline and $H_2Ti_3O_7$ silver nanotubes. This figure indicates that the absorption edge has shifted to a shorter wavelength with the transformation of silver nanocrystalline materials to one-dimensional titanate nanotubes. The band-gap energy was shifted from 2.93 and 2.95 to 3.16 and 3.30, respectively (see Table 1). These increases in band-gap energy are correlated with the transformation from the tetragonal (anatase) to the monoclinic crystalline phase (trititanate $H_2Ti_3O_7$), also the lixiviation of some silver nanoparticles during 3D to 1D transformation can shift the band-gap energy.

In the visible region of the spectra, a surface plasmon resonance (SPR) was observed in the silver semiconductors within the 400–700 nm range with the exception of the Nc-STSG powder for which the SPR signal seems negligible. Such SPR absorption has also been reported for silver nanoparticles size (~5 nm) impregnated into different nanotube-based substrates [11,15]. The SPR results may be explained by the size of the silver ion effect; for example, plasmon absorption was observed for particles larger than 5 nm [15–26]. In silver nanoparticles prepared by a similar method on different hexatitanate microfibers, the plasmon absorption was observed when the silver particles grew on the supports with a low specific surface area (10 m^2/g) [26]. In the present study, it is assumed that the low specific surface area of the photodeposited nanoparticles on commercial crystalline TiO_2 (56 m^2/g) [23] favors the formation of silver nanoparticles larger than 4 nm, which may be responsible for the observed Surface Plasmon Resonance. In the case of the Nc-STSG (130 m^2/g), some silver nanoparticles of 2 nm segregate during nanotube formation and some sinterize into larger nanoparticles, also the intermediate layered structures in Nt-STSG during 1D transformation favors the SPR. Fig. 4b. UV–vis characterization confirms the presence of silver nanoparticles smaller that 5 nm on the TiO_2 nanostructures not observed by HRTEM. These nanostructures may be excited in the range of UV irradiation. Silver nanotubes seem to require less absorption step edge (Eg) than nanocrystalline structures, indicative of a band gap transition, Fig. 5.

3.4. Raman characterization

Fig. 6 shows the Raman spectra for the trititanate nanotubes and the corresponding analogue nanocrystalline anatase TiO_2. Raman spectra were recorded to further investigate the formation of one-dimensional structures. The nanocrystalline powders show

Table 1
Methyl orange dye kinetic parameters and physicochemical properties for the silver–TiO_2 nanocomposites.

Sample	Energy band gap (eV)	Surface area BET (m^2/g)	Degradation of methyl orange dye (35 mg L^{-1})		
			$k' \times 10^{-3}$ (min^{-1})	Half-life time (min)	Mineralization (%)*
Photolysis (254 nm)	–	–	1.0	693	8.87
Nc-STSG	2.93	130	11.0	63	48.7
Nt-STSG	2.16	–	2.0	347	4.42
P25	3.16	56	6.0	116	28.2
Nc-STPD	2.95	52	13.0	53	58.2
Nt-STPD	3.30	–	1.4	495	5.17

* % of mineralization of methyl orange dye at 210 min.

characteristic active Eg modes at 144, 200, 400, 513, 525, and 640 cm^{-1} which are attributed to the Eg, B1g, A1g, B2g and Eg vibrational modes of TiO_2, respectively. These active modes indicate the presence of the anatase phase [27].

In contrast, our prepared nanotube structures have the characteristic active Eg modes of the titanate phase at 200, 278, 450, 715, 835, and 920 cm^{-1} [18]. From Raman characterization, the pure structure of the nanotubes of hydrogen trititanate remains uncertain due to the coexistence of mixed orthorhombic and monoclinic phases. The Raman spectra of the powder from the nanotubes show somewhat broader Raman bands of the titanate phase and contains additional bands at 208, 400, and 672 cm^{-1} from a possible trace amount of TiO_2 (anatase). The presence of the rutile TiO_2 phase is not detectable due to the fact that the principal mode of vibration coincides with that of the anatase mode at 144 cm^{-1}. The bands at 200 and 920 cm^{-1} are intrinsic to the hydrogen titanate phase and are suggested to be due to Ti–O–H. The as-prepared titanate structures show a negligible anatase phase content and agree well with hydrogen trititanate phase.

3.5. Photocatalytic activities of silver nanocomposites

In the photodecomposition of methyl orange dye (MOD) only silver–TiO_2 and silver-nanotubes were evaluated. All the catalysts followed pseudo-first-order kinetics and the apparent rate constant was calculated by plotting $\ln(C_0/C)$ versus time (see Table 1).

The corresponding activities are reported as half-time $t_{1/2}$ in Table 1. The photocatalytic decomposition of MOD using Nc-STSG and Nc-STPD ($H_2Ti_3O_7$) nanotubes after 210 min in irradiation photodecomposition reaches the percentages of 89 and 90%, respectively, with different behaviors (see Figure 8). For the Nt-STSG and Nt-STPD nanocrystalline samples, the photodecomposition decreases to 35% and 32%, respectively. Meanwhile, without the nanocrystalline samples, a photodegradation similar to that of the photolysis (31%) was observed (Fig. 7).

This behavior can be explained by the fact that the electronic properties of semiconductors depend on the nature and structure of defects present within their lattices. In the case of nanotubes morphology, the titanate nanotube is composed of an one-dimensional nanostructure generated from nanosheets of TiO_6 octahedra, and therefore unique photoactivable properties may be expected. Nanocrystalline TiO_2 has a tridimensional tetragonal structure where slightly distorted octahedra (octahedrally coordinated Ti atoms) are the basic building units. This anatase to hydrogen titanate phase transition induces the variation of the photoactive properties in the oxidation of MOD. In layered titanate compounds, there is a structural increase of Ti-oxygen bonded, mostly in the layered protonic titanates. Overload of oxygen in interlayered nanotubes can make difficult the transfer of interfacial charges and, at the low concentration of Ag, functionalized nanoparticles are not in sufficient concentration to accept photoinduced electrons efficiently. This is one of the reasons for the loss of activity in nanotube structures, even if the highly dispersed silver nanoparticles are smaller than 5 nm. Normally, in crystalline anatase TiO_2 phase, silver nanoparticles act as captors of photoinduced electrons, so MOD molecule is attached at the site of electron deficiency and decomposed by electron transfer. Some results suggest improved degradation of MOD with metal-doped or metal-deposited nanotube 1-D structures, as reported. Wang et al. [28] achieved complete degradation of MOD (5 mg L^{-1}) in 30 min using Ru-doped TiO_2 nanotubes as electrodes in the photocatalytic reaction with 125 W UV radiation. The application of a 0.2 V bias potential helps the interfacial transfer between the Ru-nanotubes surfaces and MOD. Degradation rate of MOD using

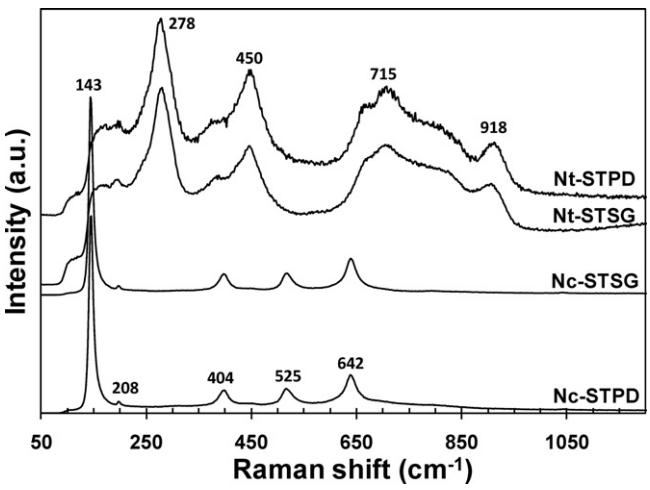

Fig. 6. Raman spectra of silver nanocrystalline and nanotube composites.

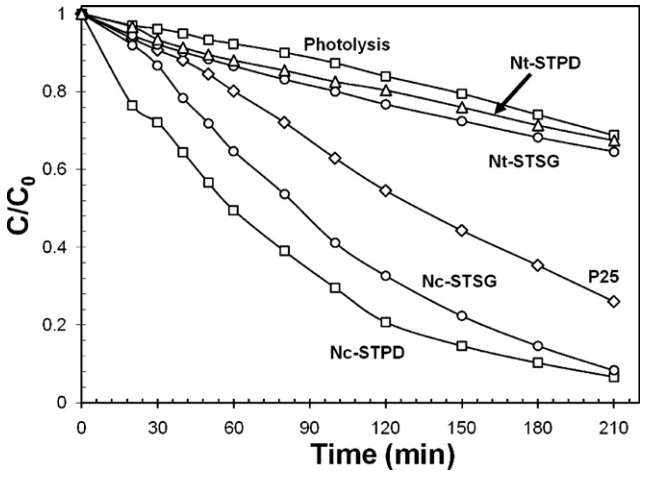

Fig. 7. Photocatalytic evolution of methyl orange oxidation under UV irradiation as a function of time.

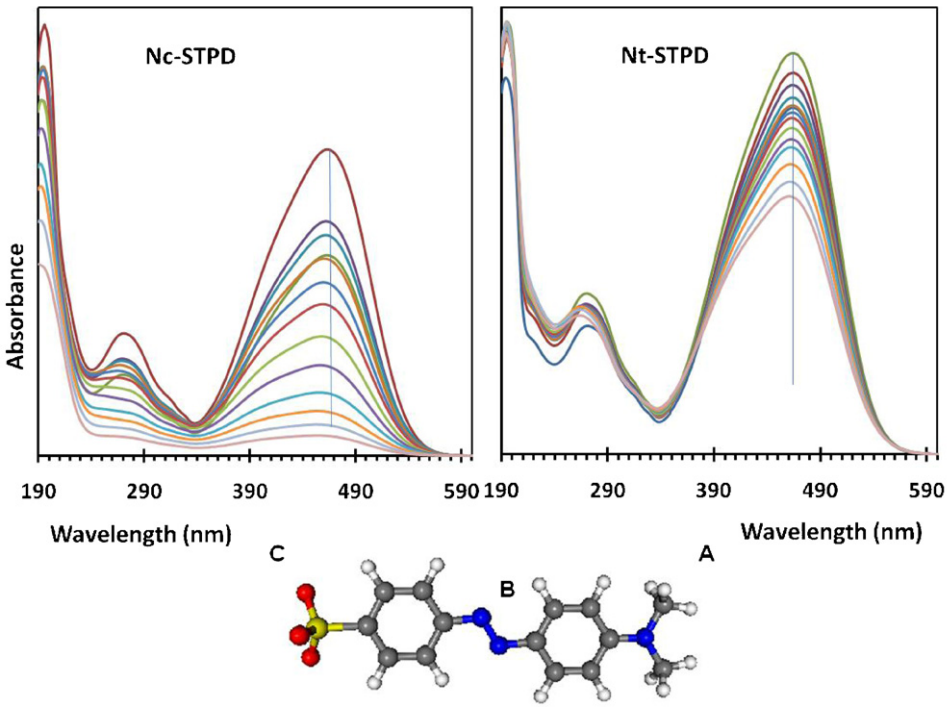

Fig. 8. UV–vis spectra correlated with molecular structure of MOD.

Ru-Doped TiO_2 nanotubes was found to be 1.33 times as high as of that using TiO_2 nanotubes. Huiqin et al. [29] investigated the effect of varying pH in the photocatalytic process using a concentration of 17 mg L^{-1} of MOD and UV-light of 300 W and iron-coated hydrogen titanate nanotubes. About 100% degradation of MOD is achieved after 1.5 h of irradiation at pH of 2.4. Acid solution tone the surface charge and H^+ ions existing in aqueous medium play an important role in photocatalytic activity, specifically in interfacial charges transfer. Our results are evidence of similar photocatalytic activity at neutral pH (7.2) and at much less powerful UV-Lamp (4400 μW/cm^2) with higher concentration of MOD (35 mg L^{-1}) with the 1-D nanotubes than reported in the previously researches and enhanced photocatalytic activity with crystalline silver–TiO_2 composites. Therefore, the studies are focused in alternative methods to increase the activity of TNTs without the undesirable effect of pore blockage to avoid the elimination of surface OH group and stabilized tube morphology with a post-thermal treatment [13].

To find the percentage of mineralization of the precursors Nc-STPD and Nc-STSG and the 1-D structures Nt-STPD and NtSTSG, an analysis of total organic carbon (TOC) in the four samples was performed with aliquots taken after 210 min of UV-light irradiation. The calculated initial TOC value is 16.8 mg L^{-1}. Accordingly, from TOC values determined for Nc-STPD slurry and Nc-STSG, the percentage of mineralization is greater compared with Nt-STPD and Nt-STSG (see Table 1). However, nanocrystalline materials reach about 50% of mineralization, while photolysis only achieves ∼9% of mineralization and commercial P25 only 28%. It is clear that the silver–titania composite increases the mineralization of MOD. The possible reasons for this improved performance may be due to the synergic effect of nanometric silver particles of 1.5 nm in diameter that inhibit the accumulation of electrons on Ag° nanoparticles, resulting in a capture of electrons that improves the quick separation of charges. These effects can enhance the UV activity on the MOD oxidation–mineralization. In contrast, hydrogen nanotubes favor oxidation rather than mineralization. It is clear that the morphology-structure is important for this photocatalytic reaction and that silver particles dispersed in nanometric size on 1-D structures do not have the same synergic effect that provides enhanced photoactivity in 3-D nanocrystalline silver–TiO_2 structures. Perhaps some silver nanoparticles are trapped in the interlayer spaces due to the TiO_6 octahedra.

To understand the interaction of MOD with silver-TiO_2 nanocristalline composites or silver hydrogen nanotubes, UV–vis spectra as a function of time were correlated with the molecular structure of MOD. Three different sites (A, B, and C) of the MOD molecule were examined (see Fig. 8). The photoassisted decomposition of MOD implies breakdown of the chromophoric groups present in the MOD molecule. In the UV–vis absorption spectra, strong absorbance at wavelengths lower than 320 nm, implies the fragmentation of the MO molecule leading to the formation of intermediate species whose degradation requires a longer reaction time [31]. The bands at 280 and 198 nm are due to the presence of the benzene rings in the molecule. MOD is characterized by a band in the range 330–560 nm in the visible region attributed to the azo functional group (shown in Fig. 8). Under progressive protonation, the color of the solution changes from orange-yellow to red due to the formation of the mono protonated form of MOD, which exists as the resonance hybrid pair with the quine diamine and azonium structures [31].

Degradation of MOD occurs by a N-demethylation mechanism [30,31]. The N-demethylation of the MOD dye takes place by a stepwise mechanism with various N-demethylated and protonated intermediate species. This N-demethylation is responsible for the slight hyposochromic shifts of the main absorption band from 463 to 454 nm. The N-demethylation process continues until the formation of the completely N-demethylated dye. In addition, the methyl groups are removed one by one, as can be confirmed by the gradual wavelength shifts of the maximum-peaks toward the blue region [30]. In Fig. 8, we compare UV–vis absorption spectra evolution as a function of time for the MOD photodecomposition over or attached to the prepared Nc-STPD and Nt-STPD semiconductors. In nanocrystalline structure Nc-STPD, the degradation requires a short reaction time to complete N-demethylation and breakage of

the azo bonds. Then the benzene intermediaries start to decompose to achieve complete decomposition of MOD. In agreement with the electronic density surface of MOD, methyl orange is probably simultaneously attacked at the azo bond (site B in Fig. 8) and at the N-demethylation (site A in Fig. 8). The benzene ring is decomposed or the benzene groups are liberated and benzene intermediates are generated. The site C (see Fig. 8) is subsequently attacked, but due to the presence of sulfur it is the most difficult part of the molecule to decompose. In silver-nanotube structures the crucial step that limits decomposition is the breakdown of the azo group, probably due to the layered titanate structure with excess of oxygen impeding the transfer of photo-electrons generated by the UV irradiation. As is shown in Fig. 7, the photocatalytic oxidation behavior of MOD may generate fewer intermediates on silver–TiO_2 structures than on silver-nanotubes. The trititanate nanotubes are interesting due to the existence of one-dimensional nanoscale channels, the interlayer spaces and silver nanoparticles coexistence. The possibilities of applying the obtained silver $H_2Ti_3O_7$ are under investigation.

4. Conclusions

$H_2Ti_3O_7$ nanotubes from silver nanocrystalline TiO_2 were successfully synthesized via a hydrothermal method using microwave irradiation in only 4 h. The presence of Ag° nanoparticles in the precursor causes the rapid and more completed formation of layered $H_2Ti_3O_7$ nanotubes compared to bare TiO_2 precursor. The cylinder-like multi-walled titanate nanotubes of both precursors have diameters of 8–10 nm and lengths of a few microns. Tubes tended to agglomerate forming bundles. All obtained tubes were open-ended. UV–vis characterization confirms the presence of small (∼5 nm) silver nanoparticles on the 1-D nanostructures. These nanostructures have broad and intense absorptions between ∼180 and 570 nm of the UV–vis region of the spectrum. Silver trititanate nanotubes requires less absorption at the step edge (Eg) than the nanocrystalline structure, indicative of a band gap transition. Silver nanoparticles dispersed on the surface of 1-D or 3-D structures with similar size (∼4 nm) can act as captors of electrons. However, it is clear that the morphology-structure is important for the photocatalytic oxidation of methyl orange dye and that the dispersed silver nanoparticles over 1-D structures (monoclinic) do not allow the same synergic effect that enhances photoactivity in 3-D nanocrystalline silver–TiO_2 structures (tretagonal structure). As-synthesized nanocrystalline materials attain about 50% of mineralization and 90% of oxidation of MOD, while photolysis only achieves about 9% of mineralization, and commercial P25 only 28%. The activities showed for 1-D silver–$H_2Ti_3O_7$ nanotubes are similar to those reported in the literature.

Acknowledgment

This work was supported by the Development of Multifunctional Nanomaterials and Processing Technology for Eco-friendly Applications from The National Research Foundation of Korea. We thank Gladis Labrada Delgado and Nicolas Cayetano Castro of LINAN-IPICYT, for the FESEM-Raman and HRTEM characterization of the materials studied in this work.

References

[1] H. Zhu, Y. Lan, X.P. Gao, S.P. Ringer, Z.F. Zheng, D.Y. Song, J.C. Zhao, J. Am. Chem. Soc. 127 (2005) 6730–6736.
[2] Oppenläder, Photochemical Purification of Water and Air. Advanced Oxidation Processes (AOPs): Principles, Reaction Mechanisms, Reactor Concepts, Wiley-VCH, 2003.
[3] A. Fujishima, T.N. Rao, D.A. Tryk, J. Photochem. Photobiol. C 1 (2000) 1–21.
[4] G.L. Puma, P.L. Yue, Environ. Sci. Technol. 33 (1999) 3210–3216.
[5] D. Li, W. Dong, S. Sun, Z. Shi, S. Feng, J. Phys. Chem. C 112 (2008) 14878–14882.
[6] S.E. John, S.K. Mohapatra, M. Misra, Langmuir 25 (2009) 8240–8247.
[7] Y.R. Smith, A. Kar, V.R. Subramanian, Ind. Eng. Chem. Res. 48 (2009) 10268–10276.
[8] T. Shokuhfar, G.K. Arumugam, P.A. Heiden, R.S. Yassar, C. Friedrich, ACS Nano 3 (2009) 3098–3102.
[9] K. Nagaveni, G. Sivalingam, M.S. Hegde, G. Madras, Environ. Sci. Technol. 38 (2004) 1600–1604.
[10] V. Rodríguez-González, R. Gómez, M. Moscosa-Santillan, J. Amouroux, React. Kinet. Catal. Lett. 90 (2007) 331–338.
[11] J.A. Toledo-Antonio, M.A. Cortes-Jácome, C. Angeles-Chavez, E. López-Salinas, P. Quintana, Langmuir 25 (2009) 10195–10201.
[12] M.A. Khan, H.T. Jung, O.B. Yang, J. Phys. Chem. B 110 (2006) 6626–6630.
[13] H.-H. Ou, S.-L. Lo, Sep. Sci. Technol. 58 (2007) 179–191.
[14] S. Nosheen, F.S. Galasso, S.L.B. Sui, Langmuir 25 (2009) 7623–7630.
[15] F. Cesano, S. Bertarione, M.J. Uddin, G. Agostini, D. Scarano, A. Zecchina, J. Phys. Chem. C 114 (2010) 169–178.
[16] D. Wu, Y. Chen, Y. Liu, X. Zhao, A. Li, N. Ming, Appl. Phys. Lett. 87 (2005) 112501.
[17] G. Guo, B. Yub, P. Yuc, X. Chen, Talanta 79 (2009) 570–575.
[18] T. Gao, H. Fjellvag, P. Norby, Inorg. Chem. 48 (2009) 1423–1432.
[19] M. Gateshki, Q. Chen, L.M. Peng, P. Chupas, V. Petkov, **Z. Kristallogr.** 222 (2007) 612–616.
[20] Y.Q. Wang, G.Q. Hu, X.F. Duan, H.L. Sun, Q.K. Xue, Chem. Phys. Lett. 365 (2002) 427–431.
[21] S.K. Pradhan, Y. Mao, S.S. Wong, P. Chupas, V. Petkov, Chem. Mater. 19 (2007) 6180–6186.
[22] H.Y. Zhu, Y. Lan, X.P. Gao, S.P. Ringer, Z.F. Zheng, D.Y. Song, J.C. Zhao, J. Am. Chem. Soc. 127 (2005) 6730–6736.
[23] V. Rodríguez-González, S.O. Alfaro, L.M. Torres-Martínez, S.H. Cho, S.W. Lee, Appl. Catal. B 98 (2010) 229–234.
[24] Q. Chen, W. Zhou, G.H. Du, L.M. Peng, Adv. Mater. 14 (2002) 1208–1211.
[25] X.D. Meng, D.Z. Wang, J.H. Liu, S.Y. Zhang, Mater. Res. Bull. 39 (2004) 2163–2170.
[26] V. Rodríguez-González, M.A. Ruiz-Gómez, L.M. Torres-Martínez, R. Zanella, R. Gómez, Catal. Today 148 (2009) 109–114.
[27] W. Ma, Z. Lu, M. Zhang, Appl. Phys. A 66 (1998) 621–627.
[28] L. Wang, Y. Binghua, 2010 4th International Conference on Bioinformatics and Biomedical Engineering (iCBBE), 2010, p. 1, doi:10.1109/ICBBE.2010.5514829.
[29] H. An, J. Li, J. Zhou, K. Li, B. Zhu, W. Huang, J. Mater. Chem. 20 (2010) 603–610.
[30] V. Rodríguez-González, X.L. García-Montelongo, L.L. Garza-Tovar, S.W. Lee, L.M. Torres-Martínez, Res. Chem. Intermed. 35 (2009) 187–196.
[31] G.L. Devi, K.M. Reddy, Appl. Surf. Sci. 256 (2010) 3116–3121.